

Analyst

Accepted Manuscript



This is an *Accepted Manuscript*, which has been through the Royal Society of Chemistry peer review process and has been accepted for publication.

Accepted Manuscripts are published online shortly after acceptance, before technical editing, formatting and proof reading. Using this free service, authors can make their results available to the community, in citable form, before we publish the edited article. We will replace this *Accepted Manuscript* with the edited and formatted *Advance Article* as soon as it is available.

You can find more information about *Accepted Manuscripts* in the [Information for Authors](#).

Please note that technical editing may introduce minor changes to the text and/or graphics, which may alter content. The journal's standard [Terms & Conditions](#) and the [Ethical guidelines](#) still apply. In no event shall the Royal Society of Chemistry be held responsible for any errors or omissions in this *Accepted Manuscript* or any consequences arising from the use of any information it contains.

EDGE ARTICLE

Methane–oxygen electrochemical coupling in an ionic liquid: a robust sensor for simultaneous quantification

Cite this: DOI: 10.1039/x0xx00000x

Zhe. Wang,^a Min. Guo,^a Gary A. Baker,^b J. Stetter,^c Lu Lin,^a Andrew J. Mason^d and Xiangqun Zeng^{*a}Received 00th May 2014,
Accepted 00th May 2014

DOI: 10.1039/x0xx00000x

www.rsc.org/

Current sensor devices for the detection of methane or natural gas emission are either expensive and have high power requirements or fail to provide a rapid response. This report describes an electrochemical methane sensor utilizing a non-volatile and conductive pyrrolidinium-based ionic liquid (ILs) electrolyte and an innovative internal standard method for methane and oxygen dual-gas detection with high sensitivity, selectivity, and stability. At a platinum electrode in bis(trifluoromethylsulfonyl)imide (NTf₂)-based ILs, methane is electro-oxidized to produce CO₂ and water when an oxygen reduction process is included. The *in-situ* generated CO₂ arising from methane oxidation was shown to provide an excellent internal standard for quantification of the electrochemical oxygen sensor signal. The simultaneous quantification of both methane and oxygen in real time strengthens the reliability of the measurements by cross-validation of two ambient gases occurring within a single sample matrix and allows for the elimination of several types of random and systematic errors in the detection. We have also validated this IL-based methane sensor employing both conventional solid macroelectrodes and flexible microfabricated electrodes using single- and double-potential step chronoamperometry.

Introduction

Methane is one of the most abundant and relevant gases on earth. The clear hazards posed by methane bring urgency to the development of an inexpensive methane sensor that is stable, reliable, highly sensitive, and selective whilst being operable in a wide variety of environmental settings with minimal power requirements and maintenance¹⁻³. Methane is typically detected by heated catalytic beads (*i.e.*, a pellister, consists of a specially-matched pair of precision resistive thermal devices), heated metal oxides (HMOx), or non-dispersive infrared instruments (NDIR), each with its own limitations. Most importantly, the cost and power required for each of these approaches precludes them from widespread deployment in mines, industrial factories, fence-lines or pipelines, homes, and other common environments where methane/natural gas is employed. Furthermore, the high power requirement is incompatible with modern wireless technologies that are capable of operating for years from a single non-recharged battery or a computer USB port. To address these shortcomings, new methane-monitoring technology is needed that can perform real-time detection and analysis at low cost employing a miniaturized sensor device. Sensors based on electrochemical transduction have clearly emerged as lead

candidates for miniaturization, offering minimal power consumption at a cost practical for mass production and commercialization. Electrochemical methods also enable real-time *in-situ* measurement without requiring periodic sampling and they have proven effective for measuring numerous trace airborne targets such as CO, CO₂, NO, NO₂, SO₂ and O₂.⁴⁻⁷ While the electrochemical oxidation of methane is thermodynamically favorable, it is kinetically slow. In order to obtain an appreciable rate of electrooxidation for methane, hot acid electrolytes (at 80 to 180 °C) must generally be employed with a platinum (Pt) electrocatalyst.^{8,9} Not only do aqueous and corrosive acid electrolytes require complex sensor architectures to prevent solvent losses, but the incomplete oxidization of methane also generates CO byproduct which poisons the Pt electrode after a few uses in these electrolytes.¹⁰⁻¹² Furthermore, methane oxidation products can accumulate at the electrode surface, limiting the sustainable operation of the sensor. Because the selectivity of an electrochemical sensor is often based on the value of the working electrode potential, an individual sensor is frequently unable to provide adequate selectivity for analyte detection in real world scenarios where interfering species may be present or perhaps even abundant.¹³ Traditionally, sensor arrays are used to address this

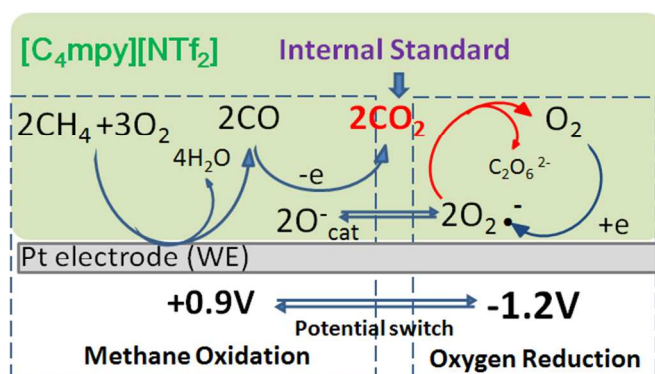
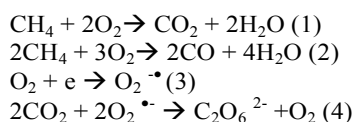


Fig. 1 Overall scheme for methane oxidation and coupled oxygen reduction in $[C_4mpy][NTf_2]$. In this approach, methane detection is based on its oxidation and oxygen is quantified by its reduction process using the *in-situ* generated CO_2 as an internal standard. Employing this strategy, the product of incomplete methane oxidation (CO) is oxidized by active oxygen species. CO_2 is used to calibrate the oxygen concentration by a coupling reaction with superoxide.

shortcoming, however, this necessarily adds to the cost and complexity of the sensor system.

We have recently discovered that, at a Pt electrode in bis(trifluoromethylsulfonyl)imide (NTf_2)-based ILs, methane is electro-oxidized to produce CO_2 and water at room temperature when an oxygen reduction process was included.¹⁴ As shown in figure 1, methane can be oxidized to CO_2 and H_2O on the platinum electrode at 0.9V in $[C_4mpy][NTf_2]$ (i.e. reaction (1)). Like in other electrolytes, the incomplete reaction of reaction (2) may occur on the working electrode as well. Similar to those reported in the literature in other electrolytes, the incomplete methane oxidation reaction such as reaction (2) may occur at the working electrode which will lead to CO. In our case, due to the presence of superoxide, CO can be further oxidized by the superoxide to make CO_2 . It noted that excess superoxides can reaction with CO_2 stoichiometrically as reaction (4). Thus the distinctive electrochemically-coupled reaction taking place between stabilized $O_2^{\bullet-}$ and CO_2 not only facilitates the complete oxidation of methane but also *in-situ* removal of the product CO_2 from the electrode interface".



Ionic liquids (ILs) offer several prominent benefits as non-volatile and stable electrolytes and solvents for electrochemical gas sensors that are operable in harsh environments.¹⁵ In the present study, we demonstrate that this unique coupling chemical reactivity of superoxide produced from oxygen reduction with CO_2 generated by methane oxidation occurring within $[C_4mpy][NTf_2]$ at room temperature allows us to establish an innovative electrochemical internal standard approach for simultaneous methane and oxygen detection. Under ambient conditions, the emission of any new gaseous species will lead to a reduction of oxygen concentration. Thus, a measure of oxygen concentration is an indicator for the introduction of new gaseous species. The fact that methane oxidation and oxygen reduction within $[C_4mpy][NTf_2]$ occur at

well-separated potentials makes possible the detection of both ambient gases (i.e., CH_4 and O_2) within the same sample matrix in real time. Significantly, this new analytical method and approach has the potential to eliminate many sources of random and systematic error in the detection and increases the reliability of the measurements via cross-validation occurring for a single sensory element. We have validated this novel approach for the quantification of both methane and oxygen, employing both conventional solid macroelectrodes and interdigitated electrodes (IDE) microfabricated on the flexible Teflon by single- and double-potential step chronoamperometry (Fig. S1). It is very important to stress that this coupled chemical reactivity is made possible only by the unique features of the IL milieu,^{16, 17} and has no direct analog in conventional (e.g., aqueous) electrolytes. The ability to tailor the IL chemistry, coupled with the unique combination of features they bring, offers a fantastic opportunity for new organoelectrochemistry in the advancement of electrochemical gas sensors resilient for unconventional or extreme environments (i.e., elevated temperature, low pressure) and in the presence of complex or potentially-interfering substances (e.g., high humidity, proximity to pyrophoric materials).¹⁶ There are also prospects for miniaturization toward integration into wearable sensors adapted to the needs and limitations of real world problems.

Results and discussion

Methane–oxygen redox coupling reactions in an ionic liquid

Fig. 2 and Fig. S3A present cyclic voltammograms (CVs) of methane oxidation and oxygen reduction in $[C_4mpy][NTf_2]$ electrolyte at a Pt electrode using a modified Clark-type cell equipped with a macroelectrode (see Fig. S1A of the Electronic Supplementary Information, ESI[†]). The peak at around 0.5 V is due to PtOx and peaks at 0.8–1.0 V are due to methane oxidation. Peaks near -1.2 V arise from oxygen reduction and are associated with superoxide ($O_2^{\bullet-}$) radical formation.¹⁸⁻²¹ $O_2^{\bullet-}$ is highly reactive and may form ion-pairs with IL cations and, subsequently, redox products. However, we note that while $[NTf_2]^-$ anions provide for high anodic electrolyte stability,²²⁻²⁵ the fully-saturated bonds within pyrrolidinium (i.e., a cyclic quaternary ammonium) cations imparts excellent cathodic stability to the IL as well. Thus, $[C_4mpy][NTf_2]$ displays a higher total electrochemical stability (i.e., wide electrochemical window and electrochemical inertia) than alternate solvents.²⁶ Studies have shown that, in pyrrolidinium-based IL, $O_2^{\bullet-}$ is significantly more stable and can be re-oxidized to oxygen at -0.7 V at the subsequent anodic scan, giving highly-reversible redox signals for the $O_2/O_2^{\bullet-}$ redox couple.^{20, 21, 27, 28} As we show in the supporting information of ref. 14, no methane oxidation occurs under pure nitrogen (N_2) background. In the presence of air and with inclusion of an oxygen reduction process, methane is fully oxidized to CO_2 and H_2O in the present of superoxide ion. Superoxide is able to quickly adsorb on the electrode surface to form the active species^{29, 30} and $[C_4mpy][NTf_2]$ is one of the best solvents for stabilizing superoxide.^{20, 28, 31} Fig. S3 shows that the methane oxidation current is much smaller when the O_2 redox processes are not concurrently present, further confirming that the presence of $O_2^{\bullet-}$ facilitates the complete oxidation of methane to CO_2 and water in $[C_4mpy][NTf_2]$.^{30, 32}

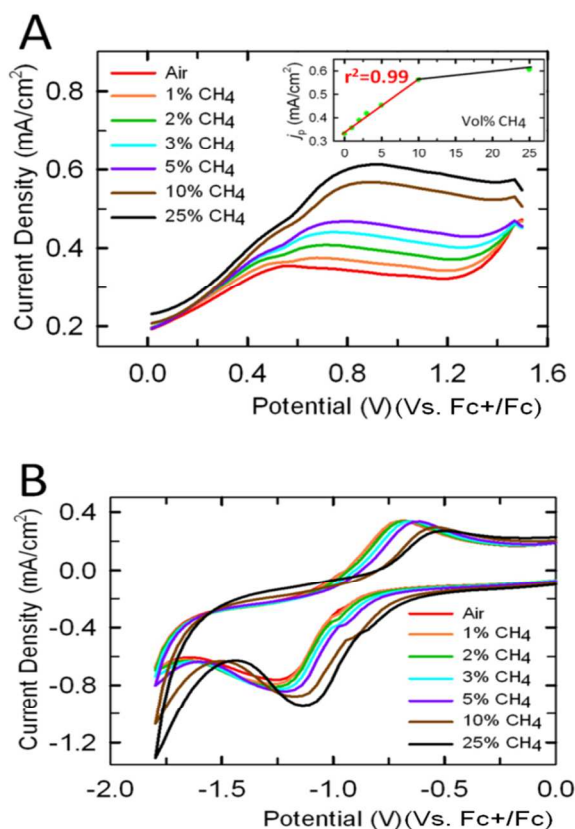


Fig. 2 Peak current density vs. potential curves at different methane concentrations in [C₄mpy][NTf₂] at a Pt electrode. (A) Methane anodic current density curves. The inset plot shows the peak current at 0.9 V against vol. % CH₄. (B) Voltammograms measured in the oxygen reduction potential window. Scan rate: 500 mV s⁻¹; potentials are referenced to the Fc⁺/Fc couple (Electronic supporting information. 1.2)

CO₂ reacts with O₂⁻ readily in an IL.^{19, 33-36} However, the reaction of water with O₂⁻ is very slow in the aprotic IL used in this study³⁷ (see Fig. S4 and S5). Since [C₄mpy][NTf₂] is hydrophobic, the water produced during methane oxidation should primarily remain at the electrode surface. Some H₂O may also be removed from the system by carrier gas flow. The traces of H₂O on the Pt electrode surface may react with Pt-O to form Pt-OH and the surface-bonded OH constitutes the oxygen donor reacting with surface-bonded CO to form CO₂.³⁸ Due to the hydrophobicity of [C₄mpy][NTf₂], the amount of water dissolved within the bulk [C₄mpy][NTf₂] is, however, essentially negligible in these experiments. (Table S2) Thus, superoxide reacts predominantly with CO₂ rather than with water. As shown in Fig. 2B, the cathodic currents for oxygen reduction increase, and both the oxygen reduction peak potential and the O₂⁻ oxidation peak potential shift to more positive values with increasing methane concentration. The shoulder peak at -0.8V appears only after the second CV cycle, in line with the coupling chemical reaction between the methane oxidation product CO₂ and the O₂⁻. The rate of methane oxidation is determined by the rate of product (*i.e.*, CO₂) depletion from the electrode. However, CO₂ may catastrophically lower the rate of oxidation at Pt by generating

CO which poisons the electrode; *viz.*, CO₂ + 2Pt-H → Pt-CO + H₂O + Pt.³⁹ The distinctive electrochemically-coupled reaction taking place between stabilized O₂⁻ and CO₂^{18, 36, 37} not only facilitates the complete oxidation of methane but also *in-situ* removal of the product CO₂ from the electrode interface.

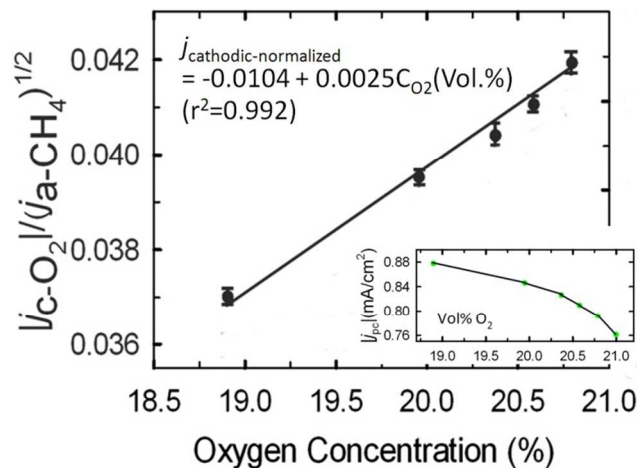


Fig. 3 Normalized oxygen cathodic peak current densities (*j*) at -1.2V using the internal standard signal from CH₄ as a function of vol% oxygen. Inset: a plot of the non-normalized results.

As shown in reactions (3) and (4), the coupled CO₂ reaction with O₂⁻ is a typical EC' reaction (electrode reaction followed by catalytic reaction)⁴⁰ in which a non-electroactive species (CO₂) reacts with O₂⁻ to regenerate reactant O₂.^{40, 41} The peroxodicarbonate (C₂O₆²⁻) generated from reaction (4) involves multiple steps.⁴² Thus, the fate of C₂O₆²⁻ within ILs is not presently known. In our experiments, we did not observe interference from C₂O₆²⁻ in the methane signal over 120 days. Therefore, the amount of C₂O₆²⁻ produced is either dissolved into the bulk fluid or its interface concentration is too low to substantially impact the sensory signals. The solubility of CO₂ in [C₄mpy][NTf₂] is low and our results show that CO₂ present in the ambient environment does not affect the distinctive electrochemically-coupled reactions taking place at the electrode interface. As such, the *in-situ* generated CO₂ resulting from methane oxidation is the predominant CO₂ taking part in the reaction(s) at the interface. In the following discussion, we establish that the CO₂ generated from methane oxidation is an excellent internal standard for electrochemical quantification of oxygen in the ambient environment. The internal standard method involves the use of a well-behaved compound (*i.e.*, a known substance that is absent from the sample matrix) that is added in a constant amount to all samples (*e.g.*, blanks, calibration standards, samples) during an analysis. The calibration generally involves calculating the ratio of the analyte signal to that from the internal standard compound, and then plotting this ratio as a function of the analyte concentration. The main difficulty in this approach involves the identification of a suitable substance to serve as the internal standard and to add it to the samples and standards in a reproducible manner such that analyte and internal standard signals both respond proportionally to the random and instrumental fluctuations as well as the sample matrix effects, in order to compensate for errors. The *in-situ* generated CO₂ formed via methane electrooxidation in [C₄mpy][NTf₂] at room temperature serves as an ideal internal standard, enabling the highly accurate measurement of methane and oxygen in a single electrochemical sensor.¹⁴ The internal standard

method allows for the calibration of many types of random and systematic errors, a highly desirable feature for robust chemical analysis. The current of this EC' reaction can be described by eq. (5):

$$j_{\text{O}_2\text{-cathodic}} = \frac{nFC_{\text{O}_2}^*(Dk'C_{\text{CO}_2}^*)^{1/2}}{1 + \exp\left[\frac{nF}{RT}(E - E_{1/2})\right]} \quad (5)$$

Here, D is the diffusion coefficient, C^* is the concentration of gas in the liquid phase, k' is the rate constant of reaction (3), and E is the potential. The oxygen reduction currents are related to both of the oxygen concentration and the square root of CO_2 concentration.



The concentration of CO_2 is dominated by the methane oxidation process; *i.e.*, $[\text{CO}_2]$ is linearly correlated with the methane anodic current:

$$C_{\text{CO}_2}^* \propto j_{\text{CH}_4\text{-anodic}} \quad (6)$$

The analyte (CH_4 and O_2) concentrations at ambient conditions are inter-related due to a constant ambient pressure. Changes in the oxygen concentration do not affect signal intensities for methane at low methane concentrations since oxygen is present in excess. From 0–10 vol%, the calibration curve for methane detection using our sensor is as follows:

$$j_{(0-10\%)} (\text{A}/\text{cm}^2) = 2.27 \times 10^{-5} (\text{A}/\text{cm}^2\%) \times C_{\text{CH}_4} (\text{vol}\%) + 3.38 \times 10^{-4} (\text{A}/\text{cm}^2) \quad (r^2 = 0.992) \quad (7)$$

Thus, the methane sensitivity is $22.7 \mu\text{A}/\text{cm}^2\%$, while the sensitivity drops at high methane concentration. The stoichiometric ratio of methane to oxygen is 1:2. Since we used air as our background gas, 21% oxygen is the maximum concentration of oxygen in air. For methane concentrations higher than 10%, methane oxidation becomes limited by the oxygen concentration and the slope of the sensitivity decreases, as shown in the Fig. 2A insert.

As shown in the Fig. 3 insert, the oxygen reduction peak current follows a nonlinear relationship with oxygen concentration. However, according to eq. (5) and (6) the $j_{\text{O}_2\text{-cathodic}}$ can be normalized by the square root of $j_{\text{CH}_4\text{-anodic}}$. The calibration curve constructed by plotting the ratio of the oxygen reduction peak current normalized to the square root of the methane anodic peak current as a function of oxygen concentration is linear, demonstrating the feasibility of the internal standard method. In the 1–10 vol% methane range (over which the corresponding oxygen concentration goes from 21 to 19 vol%), the linear relationship between the oxygen concentration and peak current is given in Fig. 3; the concentration of oxygen can be determined using the expressions given in Fig. 3.

Methane–oxygen redox coupling reaction for dual-gas quantification

For practical electroanalytical applications, potential-step (*i.e.*, chronoamperometry) methods are the simplest to employ. Fig. 4A displays chronoamperograms for methane oxidation at different methane concentrations using the two electrodes illustrated in Fig. S1, a Pt gauze pressed onto a porous Teflon membrane and a microfabricated planar Pt electrode on a flexible Teflon gas-permeable membrane. As shown in Fig. S6, the time constant (τ , the time required for current to decay to its $1/e$ value; *i.e.*, $\sim 37\%$ of the maximum current) obtained from a

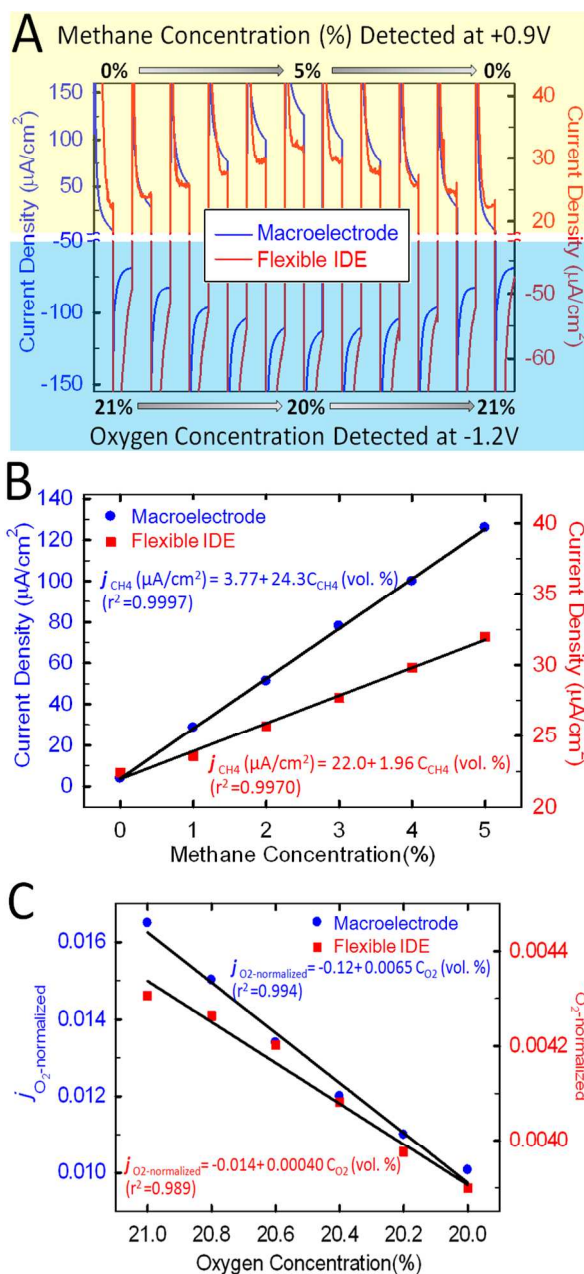


Fig. 4 (A) Real-time results for methane oxidation at 0.9 V and oxygen reduction at -1.2 V by double-potential step chronoamperometry. The DC potential was switched between 0.9 V and -1.2 V at each concentration. Current density transients were recorded in response at the two switched potentials to stepwise 1% changes in methane concentration. Two different electrodes were used: a Pt gauze macroelectrode (blue symbols/curves) and a flexible Pt interdigitated electrode (red symbols/curves). The time interval was 300 s for each potential step. (B) Plots of methane anodic current density at 0.9 V applied vs. methane concentrations. (C) Plots of normalized oxygen reduction current density at -1.2 V vs. oxygen concentration. Note: we deliberately reversed oxygen concentration in order to be consistent with Fig. 4B, in which methane concentration increased with a concomitant decrease in oxygen concentration.

potential step experiment (from 0.0 V to 0.9V in 100% air) is 6 s. In order to minimize the double layer charging current,^{38, 48} we measured the methane oxidation or oxygen reduction current at 300th (50τ) second. The double layer charging current is negligible at 50τ and the current can be largely attributed to faradaic current. The same program was repeated 11 times at different methane concentrations ranging from 0 to 5 vol.% in air. Highly reproducible current responses were obtained as a result. The methane concentration can thus be quantified directly by anodic current at 0.9 V and oxygen concentration determined from the internal standard method discussed above. Higher sensitivity was obtained from the macroelectrode versus the planar interdigitated electrode, because of its 3-D structure and the highly activated Pt gauze surface. The microfabricated planar Pt electrode patterned on the Teflon membrane, however, is much more suitable for low-power, inexpensive, and wearable sensor platforms. The thin IL film shows excellent adherence to the Teflon substrate, taking full advantage of the high fluid viscosity. In fact, this electrode was shown to remain functional even when bent, allowing it to be pasted onto arbitrarily-shaped substrates and easily integrated into other devices.

Fig. 5A (red curve) provides a real-time response of the IL-based chronoamperometric sensor to single, stepwise increases and decreases in methane concentrations in the 0 to 5 vol% range. In this way, the current change is quantitative and reproducible upon the addition of methane or the removal of methane at each step, indicating the stability of the electrode surface and the repeatability of the measurement. The response time to achieve 80% of the maximal response (T_{80}) was determined to be ~ 13 s based on the results given in Fig. 5A. It is worth noting that this response time is convolved with gas mixing and mass flow controller operation, so it represents the upper limit of T_{80} . The dose-dependent relationship is shown in equation (8) which is nearly identical to the double-potential step chronoamperometry results shown in Fig. 4B.

$$j_{(0-5\% \text{ methane})} (\text{A}/\text{cm}^2) = 3.77 \times 10^{-6} (\text{A}/\text{cm}^2) + 2.42 \times 10^{-5} (\text{A}/\text{cm}^2\%) \times C_{\text{CH}_4} (\text{vol}\%) \quad (r^2 = 0.9997) \quad (8)$$

The IL-electrolyte electrochemical sensors based on methane oxidation and oxygen reduction described here are highly selective because the redox chemistry is a unique characteristic of the methane and oxygen target analytes. The dissolution of interfering gases in traditional aqueous electrolyte solution generates the variability of the signal. In contrast, in the present case the solubility of other gases can be controlled by judicious IL selection to minimize such interference. We selected the well-studied hydrophobic IL [C₄mpy][NTf₂] in part because the solubilities for many interfering gases is known to be low in this IL and because it is chemically inert against those interfering species so that the electrolyte content remains stable during long-term operation. Additionally, the high thermal and chemical stability of ILs makes it easier to regenerate the electrolyte if contamination does occur. Fig. 5 presents results for methane detection in the presence of common interfering inorganic species present in the troposphere. Excellent selectivity is shown under aerobic conditions because little anodic oxidation current peak is observed for the tested interfering gases. It is significant that bulk CO₂ does not interfere with methane detection. As shown in Fig. S5, CO₂ from the atmosphere (~ 0.03 vol%) presents little interference to oxygen detection, since both CH₄ and O₂ have strong adsorption on the Pt surface,⁴³ whereas CO₂ has low solubility in [C₄mpy][NTf₂] and its adsorption onto Pt is

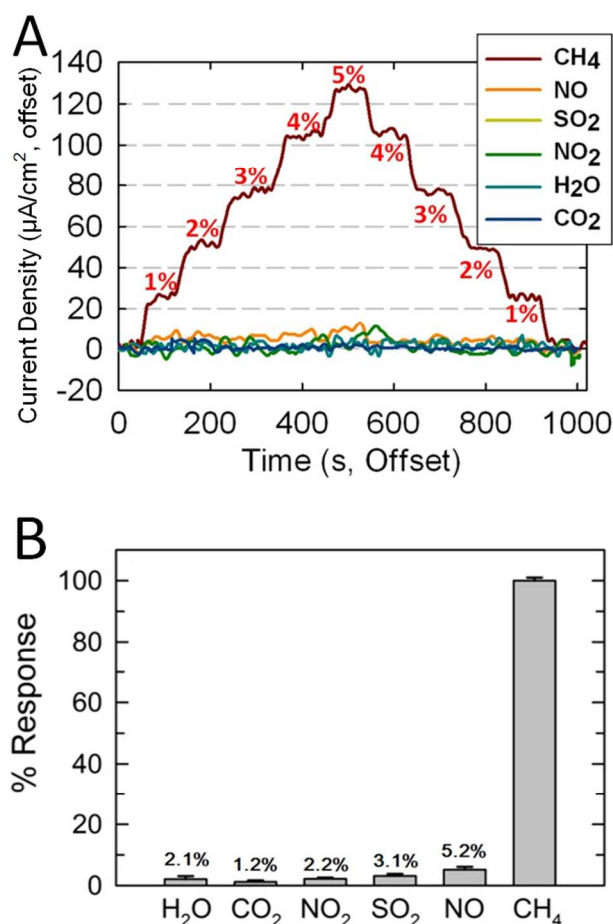


Fig. 5 (A) Current density transients recorded at 0.9 V in response to stepwise changes in methane concentration. (B) Current density response of sensor to non-target gases present at 5 vol% in air relative to 5 vol% methane in air based on the single-potential step method using a Pt gauze macroelectrode. The number appearing over each bar denotes the selectivity coefficient for methane over a given gas, based on the respective current ratio. All data were expressed as the ratio of the current change in the single-potential step chronoamperometry when 5 vol% methane or 5 vol% of the challenging gases were introduced to the sensor system. The error bars were obtained from five independent experiments for each exposure.

very low; in fact, there is no CO₂ adsorption at the PtOx surface either.⁴⁴

Both NO₂ and SO₂ are important constituents of acidic gas pollutants in the atmosphere but no oxidation peaks for either species were observed in the methane oxidation potential window giving little interference from NO₂ or SO₂. It has been reported that the presence of NO can interfere with methane oxidation under atmospheric conditions, because there is an oxidation of NO (NO to NO⁺) at positive potentials in ILs and NO is easily oxidized to NO₂.⁴⁵ Although it was difficult to observe clearly the oxidation peak of NO in [C₄mpy][NTf₂], the NO oxidation peak likely overlaps with the methane oxidation peak if they are mutually present. The influence of NO was

decreased by the presence of oxygen, likely a result of NO quickly reacting with O₂ at room temperature to form NO₂. This behavior is beneficial to our methane sensor as the methane sensor is intended for use in monitoring methane in normal atmospheric conditions where very little NO is expected to occur due to the rapid oxidation process of NO to NO₂ in the presence of large amounts of O₂.^{46, 47} For NO, NO₂, and SO₂, typical concentrations in air are very low. The maximum allowed exposure concentrations for these gases are only a few ppm in air, thus their interferences will be negligible in our intended methane sensor applications.

Methane is the most difficult hydrocarbon to be electro-oxidized. Accordingly, other hydrocarbons such as ethanol should be readily co-oxidized at potentials where methane is oxidized, giving rise to background signals. Indeed, in earlier experiments, we have observed anodic currents for hexane in [C₄mpy][NTf₂]. However, the content of flammable organic vapours such as ethanol remains very low under most methane detection conditions. Currently, the occupational standard for ethanol in air is 1000 ppm on an eight-hour basis which will generate negligible interference for methane detection. Additionally, using an IL which presents a very low solubility for potentially-interfering gases coupled with a high solubility toward methane could also improve the selectivity of the detection in more demanding and complex chemical environments. The gas-permeable Teflon membrane itself might be worth exploration as another means to provide size selectivity for solutes using controlled-pore materials. In any case, we hypothesize that the coupling chemistry that occurs between methane oxidation products and O₂^{•-} compared with that between O₂^{•-} and the oxidation product(s) of a small volatile organic compound (VOC) such as ethanol will be different. This difference might form the basis for discriminating signals and developing future strategies for even more highly selective methane detection. We are also currently exploring sensory arrays for increasing the selectivity of methane and VOC detection; such arrays can take full advantage of the tailorability of ILs by employing a palette of

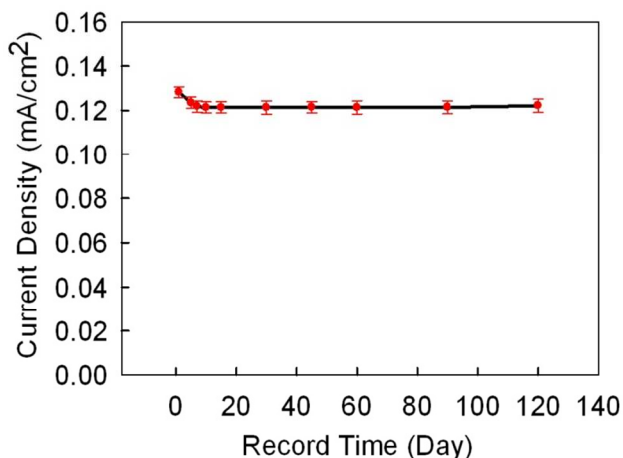


Fig. 6 Methane oxidation current measured using a Pt macroelectrode continuous 5 vol.% methane in dry air. A potential of 0.9 V was applied during the experiment and the instantaneous current was monitored continuously.

ILs for analyte discrimination.

Compared to previously-reported electrochemical atmospheric methane sensors, results to date for our [C₄mpy][NTf₂]-based methane sensor reveal very promising characteristics with good selectivity in the presence of common ambient gases, and excellent long-term stability over 120 days (Fig. 6) at room temperature.

Conclusions

In this research, we have integrated a non-volatile, conductive ionic liquid electrolyte with electrochemical transducers to introduce an innovative and high-performance methane sensor that is inherently small, low power consumption, and low cost. The unique, localized and coupled reactions (*i.e.*, the redox chemistry of oxygen and methane in [C₄mpy][NTf₂]) enable the identification/detection and quantification of both analytes using a single sensor (*i.e.*, multi-analyte discrimination without requiring a sensor array). The ionic liquid-enabled electrochemical methane sensor is shown to be specific to methane and can reliably and selectively quantify methane in the concentration range of 0.3–20 vol.% with a detection limit of 3000 ppm. The high precision and accuracy of quantitation is obtained using an internal standard strategy in which uncertainties arising from changes in the sample or the environment can be minimized or avoided. The oxygen redox process in air can also be used as a probe to evaluate electrode activity and for sensor calibration, in particular for electrocatalytic methane oxidation. Thus, within this dual-gas system, the electrode activity and gas sensitivity can be facilely calibrated by the oxygen reduction current.^{14, 21} This feature aids in eliminating false positives and false negatives by cross-validating the measurement results. This paper is the very first report of a working electrochemical methane sensor based on an ionic liquid electrolyte with an innovative dual-gas detection method. Different from other analytical systems shown earlier, methane and oxygen can be mutually calibrated using a novel internal standard method in this ionic liquid/Pt sensor. Among the analytical sciences, establishing an internal standard method using IL-mediated redox chemistry is also a first. Overall, we anticipate that the methane sensor reported herein will find significance as it increases the analytical robustness and reliability of methane detection utilizing a simple single-sensor format, holding promise for its further development toward miniaturized, low-cost, and low-power wearable sensors for industrial and domestic safety applications.

Acknowledgements

X.Z. would like to thank NIOSH R21 (Grant No. R21OH009099) and NIOSH R01 OH009644 for financial support of this work. G.A.B. acknowledges University of Missouri-Columbia start-up funds which were used partly to support the synthesis of ILs used in this study. Authors would like to thank Dr. Yirong Mo's helpful discussion

Notes and references

^a Department of Chemistry, Oakland University, Rochester, MI, US. E-mail: zeng@oakland.edu

^b Department of Chemistry, University of Missouri-Columbia, Columbia, MO, US.

^c KWJ Engineering Incorporated, 8440 Central Avenue [suite 2B or 2D], Newark, CA, US.

^d Department of Electrical and Computer Engineering, Michigan State

University, East Lansing, MI, US.

† Electronic Supplementary Information (ESI) available: experimental details, Figures S1–S6 and Table S1 described in the text. See DOI: 10.1039/b000000x/

1. Q. Schiermeier, *Nature*, 2006, **439**, 128-128.
2. G. A. Olah, G. K. S. Prakash and A. Goepfert, *J Am Chem Soc*, 2011, **133**, 12881-12898.
3. G. D. Fresch, *Planning and Environmental Law*, 2011, **63**, 3-9.
4. G. Schiavon, G. Zotti, G. Bontempelli, G. Farnia and G. Sandona, *Anal. Chem.*, 1990, **62**, 293-298.
5. A. W. E. Hodgson, P. Jacquinet and P. C. Hauser, *Anal. Chem.*, 1999, **71**, 2831-2837.
6. R. Knake, P. Jacquinet and P. C. Hauser, *Analyst*, 2002, **127**, 114-118.
7. R. M. Penner, *Nat Chem*, 2010, **2**, 251-252.
8. H. D. Gesser, N. R. Hunter and C. B. Prakash, *Chem Rev*, 1985, **85**, 235-244.
9. Q. J. Zhu, S. L. Wegener, C. Xie, O. Uche, M. Neurock and T. J. Marks, *Nat Chem*, 2013, **5**, 104-109.
10. A. T. Ashcroft, A. K. Cheetham, M. L. H. Green and P. D. F. Vernon, *Nature*, 1991, **352**, 225-226.
11. F. Hahn and C. A. Melendres, *Electrochim Acta*, 2001, **46**, 3525-3534.
12. S. M. Lang and T. M. Bernhardt, *Faraday Discuss*, 2011, **152**, 337-351.
13. N. S. Lawrence, *Talanta*, 2006, **69**, 385-392.
14. Z. Wang and X. Zeng, *J Electrochem Soc*, 2013, **160**, H604-H611.
15. G. A. Baker, S. N. Baker, S. Pandey and F. V. Bright, *Analyst*, 2005, **130**, 800-808.
16. M. Armand, F. Endres, D. R. MacFarlane, H. Ohno and B. Scrosati, *Nat Mater*, 2009, **8**, 621-629.
17. W. Lu, A. G. Fadeev, B. H. Qi, E. Smela, B. R. Mattes, J. Ding, G. M. Spinks, J. Mazurkiewicz, D. Z. Zhou, G. G. Wallace, D. R. MacFarlane, S. A. Forsyth and M. Forsyth, *Science*, 2002, **297**, 983-987.
18. I. M. AlNashef, M. L. Leonard, M. C. Kittle, M. A. Matthews and J. W. Weidner, *Electrochem Solid St*, 2001, **4**, D16-D18.
19. M. C. Buzzeo, O. V. Klymenko, J. D. Wadhawan, C. Hardacre, K. R. Seddon and R. G. Compton, *J Phys Chem A*, 2003, **107**, 8872-8878.
20. R. G. Evans, O. V. Klymenko, S. A. Saddoughi, C. Hardacre and R. G. Compton, *J Phys Chem B*, 2004, **108**, 7878-7886.
21. Z. Wang, P. Lin, G. A. Baker, J. Stetter and X. Zeng, *Anal Chem*, 2011, **83**, 7066-7073.
22. F. Endres and S. Z. El Abedin, *Physical Chemistry Chemical Physics*, 2006, **8**, 2101-2116.
23. S. J. Zhang, N. Sun, X. Z. He, X. M. Lu and X. P. Zhang, *J Phys Chem Ref Data*, 2006, **35**, 1475-1517.
24. H. P. Wang, W. W. Liu, L. Y. Cheng, Y. M. Zhang and M. F. Yu, *J Mol Liq*, 2008, **140**, 68-72.
25. D. Rooney, J. Jacquemin and R. Gardas, in *Top Curr Chem*, ed. B. Kirchner, Springer Berlin / Heidelberg, 2010, vol. 290, pp. 185-212.
26. G. H. Lane, *Electrochim Acta*, 2012, **83**, 513-528.
27. C. Xiao and X. Zeng, *J Electrochem Soc*, 2013, **160**, H749-H756.
28. E. I. Rogers, X.-J. Huang, E. J. F. Dickinson, C. Hardacre and R. G. Compton, *The Journal of Physical Chemistry C*, 2009, **113**, 17811-17823.
29. I. S. Metcalfe and S. Sundaresan, *Aiche J*, 1988, **34**, 195-208.
30. G. C. Bond and D. T. Thompson, *Gold Bull*, 2000, **33**, 41-51.
31. H. N. Najm, P. H. Paul, C. J. Mueller and P. S. Wyckoff, *Combust Flame*, 1998, **113**, 312-332.
32. W. Liu and M. Flytzani-Stephanopoulos, *J Catal*, 1995, **153**, 317-332.
33. M. C. Buzzeo, O. V. Klymenko, J. D. Wadhawan, C. Hardacre, K. R. Seddon and R. G. Compton, *J Phys Chem B*, 2004, **108**, 3947-3954.
34. I. M. AlNashef, M. L. Leonard, M. C. Kittle, M. A. Matthews and J. W. Weidner, *Electrochemical and Solid-State Letters*, 2001, **4**, D16-D18.
35. I. M. AlNashef, M. L. Leonard, M. A. Matthews and J. W. Weidner, *Ind Eng Chem Res*, 2002, **41**, 4475-4478.
36. I. M. AlNashef, M. L. Leonard, M. A. Matthews and J. W. Weidner, *Industrial and Engineering Chemistry Research*, 2002, **41**, 4475-4478.
37. D. T. Sawyer and J. L. Roberts, *J. Electroanal. Chem.*, 1966, **12**, 90-101.
38. M. T. M. Koper, S. C. S. Lai and E. Herrero, in *Fuel Cell Catalysis*, John Wiley & Sons, Inc., 2008, pp. 159-207.
39. P. Stonehart and G. Kohlmayr, *Electrochim Acta*, 1972, **17**, 369-382.
40. A. J. Bard and L. R. Faulkner, *Electrochemical Methods: Fundamentals and Applications*, 1980.
41. D. S. Silvester, L. Aldous, C. Hardacre and R. G. Compton, *J Phys Chem B*, 2007, **111**, 5000-5007.
42. M. A. Casadei, S. Cesa, F. M. Moracci, A. Inesi and M. Feroci, *Journal of Organic Chemistry*, 1996, **61**, 380-383.
43. R. R. Adžić and J. X. Wang, *The Journal of Physical Chemistry B*, 1998, **102**, 8988-8993.
44. J. Sobkowski and A. Czerwiński, *Journal of Electroanalytical Chemistry and Interfacial Electrochemistry*, 1974, **55**, 391-397.
45. S.-C. Chang and J. R. Stetter, *Electroanalysis*, 1990, **2**, 359-365.
46. I. Mochida, S. Kizamori, M. Hironaka, S. Kawano, Y. Matsumura and M. Yoshikawa, *Energ Fuel*, 1994, **8**, 1341-1344.
47. J. M. Harris and S. P. Mcmanus, *Nucleophilicity*, American Chemical Society, 1987.